Available online at www.sciencedirect.com
SCIENCE DIRECT®
Journal of Non-Crystalline Solids 319 (2003) 44–56
JOURNAL OF NON-CRYSTALLINE SOLIDS
www.elsevier.com/locate/jnoncrysol

Internal friction spectroscopy in Li_2O–$2SiO_2$ partially crystallised glasses

K. Müller [a,*], N.S. Bagdassarov [a], M. James [a,1], H. Schmeling [a], J. Deubener [b]

[a] *Institut für Meteorologie und Geophysik, J.W. Goethe Universität Frankfurt, Feldbergstraße 47, Frankfurt am Main 60323, Germany*

[b] *Institut für Nichtmetallische Werkstoffe, TU Berlin, Berlin 10587, Germany*

Received 13 February 2002; received in revised form 24 October 2002

Abstract

Oscillatory torsion deformation experiments were performed on partially crystallised Li_2O–$2SiO_2$ glasses in the temperature range 350–480 °C and with frequencies between 20 and 0.002 Hz. The experiments were carried out in a torsion deformation apparatus exerting a small strain on cylindrical samples. Data obtained at varying temperatures and frequency were reduced to master plots using a normalised frequency. The frequency shift factor has been taken as a function of temperature in an Arrhenian form, yielding an activation energy of a background Q^{-1} close to the activation energy of oxygen defect diffusion ($=120$ kJ/mol). The master curves of real and imaginary components of shear modulus and internal friction indicate a stretched exponential shear stress relaxation with a an exponent of ≈ 0.45, characteristic of a broadened relaxation spectrum. The dynamic viscosity was estimated at temperatures of 470 and 480 °C. The extrapolation of dynamic viscosity to zero frequency allowed estimation of the relaxed shear viscosity. The presence of crystals increases the relaxed shear viscosity by $\approx 0.2\log(\mathrm{Pa\,s})/10$ vol.% of crystallinity. Dependence of the relative shear viscosity of partially crystallised lithium disilicate melts on crystal content is discussed.

1. Introduction

Measurements of the losses of mechanical deformation energy into heating of solid bodies or so called internal friction spectroscopy has been the a subject of numerous investigations [1]. The experimental technique dealing with internal friction measurements in a frequency domain is defined as a mechanical spectroscopy [2]. This method allows one to characterise an anelasticity of materials, when the mechanical response of a sample to an oscillatory mechanical stress has a strain with a phase delay ϕ. The phase delay between applied stress and resulted strain defines the internal friction Q^{-1} of a material or $\tan\phi = Q^{-1} = \Delta E/2\pi E$, where ΔE is the energy dissipated per cycle of deformation and E is the energy stored in a cycle of deformation [1,3]. The frequency–temperature dependence of Q^{-1} indicates the existence of peaks

* Corresponding author. Fax: +49-69 798233280.
E-mail address: kmueller@geophysik.uni-frankfurt.de (K. Müller).
[1] Present address: Department of Environmental Science, IENS, Lancaster University, Lancaster, LA1 4YQ, UK.

0022-3093/03/$ - see front matter
doi:10.1016/S0022-3093(02)01966-X

or local maximum of the internal friction at differing frequencies and temperatures, which are superimposed on the temperature background dependency of Q^{-1}. Each peak or increase of dissipation corresponds to specific relaxation mechanisms.

Silicate glasses are usually classified as 3-D network glasses, they contain as a main component SiO_2 and alkali oxides. The long history of internal friction measurements in silicate glasses has demonstrated that they possess a distribution of relaxation times [4]. The internal friction peaks as a function of frequency are much broader than a Debye peak, which were associated with the longitudinal oscillations of bridging oxygen atoms, effects of alkali and non-bridging oxygen ions [5]. For example, in Li_2O–$2SiO_2$ there is a low temperature, low frequency internal friction peak at approximately −20 °C, which corresponds to alkali ion relaxation and has an activation energy 70–100 kJ/mol [5], and a high temperature peak at ≈250 °C, associated with the relaxation of non-bridging oxygen ions, interaction between alkali ions, oxygen ions and protons in hydrogen bonded bridging positions, and having the activation energy of 120 kJ/mol [6]. The dissipation of mechanical energy in glasses is very sensitive to water dissolved in the bulk. The mechanism of high temperature mechanical damping (≈250°) is sought to arise due to increase of alkaline mobility when more protons attached to non-bridging oxygens and the second peak increases in height and shifts to lower temperature [6]. The internal friction of partially crystallised glasses is more complicated than in pure glasses. Additional relaxations appear to be due to the grain boundary diffusion [7] and sliding [8] at high crystal fractions. At moderate fractions of crystals or melt, additional modes of internal friction may be due to torsion and flexural deformation of crystals [9]. Finally, rotation and elastic interactions of crystals (defined as a metastable Bingam flow) may contribute to shear viscosity and, therefore, to the internal friction of partially crystallised melts at low crystal fraction [10,11]. Additional high temperature peaks have been observed in partially crystallised Li_2O–$2.75SiO_2$ glasses above the glass transition temperature, T_g, at ≈500 °C, which has been suggested to be due to the relaxation of melt clustering at early stage of crystal nucleation [12].

This experimental work deals with the measurement of shear-modulus and internal friction of partially crystallised Li_2O–$2SiO_2$ glasses in torsion deformation apparatus (developed by Berckhemer et al. [13]), at temperatures slightly below and above the glass transition temperature. By measuring the internal friction over a range of frequencies (20–0.002 Hz) and temperatures (350–480 °C) we addressed the question how the viscosity and viscoelastic behaviour of silicate melts are affected by the presence of crystals, and what is an appropriate model for the viscoelastic behaviour of partially crystallised silicate melts containing up to 30 vol.% of crystals.

2. Experiments

2.1. Sample preparation

The preparation of lithium disilicate glass from melted grade quartz and lithium carbonate has been described elsewhere [11]. The starting composition of glass Li_2O–$2SiO_2$ was $Li_2O \approx 33$ mol%, $SiO_2 \approx 67$ mol% (±0.4). The method of preparing glass samples with the controlled volume fraction of crystals is based on the fact that the nucleation and crystal growth processes in Li_2O–$2SiO_2$ occur at different temperature ranges (465 and 580 °C, respectively [14,15]). By varying the annealing time and temperature range, it is possible to generate partially crystallised glasses with a different proportion of $Li_2Si_2O_5$-crystals (Table 1). Three pure glass samples were primary annealed at 460 °C for 300–400 min and in a second step at 560 °C for 200 min before being cooled at a rate of ≈0.75–1 K/min (Fig. 1). This cooling rate infers a T_g of the glass matrix of ≈440 °C according to DTA measurements [16]. DSC series on lithium disilicate glasses prepared at cooling rates between 0.3 and 2 K/min indicate $T_g \approx 445$ °C [17]. According to rheological data the crystal free lithium disilicate glass prepared at cooling rate ≈2 K/min corresponds to $T_g \approx 445$ °C, when the shear viscosity at the glass transition assumed $10^{12.5}$ Pa s [10].

Table 1
Activation energies of shear stress relaxation and unrelaxed shear modulus of disilicate lithium glasses

Sample no.	Φ, volume percent of crystals	Activation energy (kJ/mol) of the scale factor for normalised frequency	$\ln(\tau_0, \text{s})$ of the scale factor	G_∞ unrelaxed shear modulus (GPa)
Glass 0	0	137 ± 18	−50.15	24.3
Glass 1	17	129 ± 13	−47.68	23.8
Glass 3	22	126 ± 16	−45.72	24.7
Glass 5	27	117 ± 10	−42.25	25.0

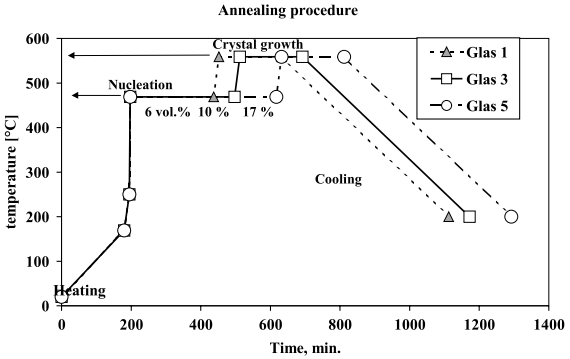

Fig. 1. Temperature profiles for preparing Li_2O–$2SiO_2$ glass samples with a fixed volume fraction of crystals 6, 10 and 17 vol.%. Depending on a differing nucleation duration, different volume fractions of lithium disilicate crystals were generated in the glass matrix. Cooling rate of all prepared samples was ≈0.75–1 K/min, corresponding to $T_g \approx 440$ °C.

The crystal content in samples was determined from quantitative microscope analysis (Table 1). The thin sections of samples were imaged using a digital camera and analysed with image processing software (Fig. 2). The lithium disilicate crystals

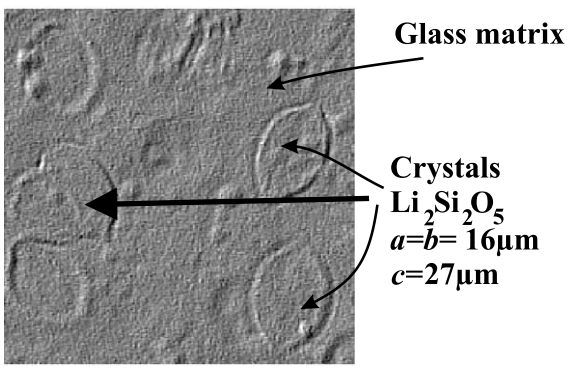

Fig. 2. Picture of Glass 5 sample in optical microscope with a magnification of 50×. The lithium disilicate crystals were oblate spheroids with aspect ratio of their axes 1:1:1.7.

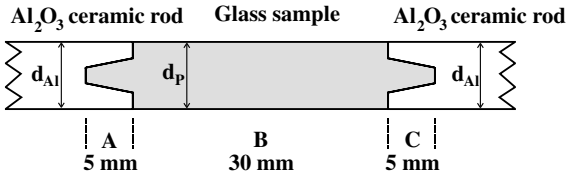

Fig. 3. Scheme of a sample fixed between two Al_2O_3-ceramic rods. Sample is machined with two conical grips on the opposite sides (angle ≈1°). Diameter of the sample d_3 and rods d_1 and d_2 is 8 mm.

have monoclinic (pseudo-orthorhombic) symmetry and are ellipsoids with an aspect ratio (*a*:*b*:*c* axes) of 1:1:1.7. The samples used for torsion experiments were machined with diamond tools to 8 mm in diameter and 30–40 mm in length. Special grips were machined on two opposite flat ends of the cylindrical samples (Fig. 3). Four samples of differing crystal content were tested (see Table 1) in the temperature range 350–490 °C and over the frequency range 2×10^{-3}–20 Hz.

2.2. Internal friction measurements

In oscillatory rheology, rheological measurements of complex shear modulus, complex shear viscosity and internal friction can be carried out over a range of frequencies. Recently developed experimental techniques to characterise the in- and out-of-phase mechanical strain under oscillating stresses (with torsional, flexural or compressional deformations) use ultrasonic attenuation [18,19], an acoustic resonator [20], inverted Kê-torsion pendulum [21,22], four-point flexural and cyclic-compression deformation [7], bending pendulum [23], or forced torsional oscillations [13,24–26].

2.3. Torsion apparatus

The equipment used here, and described in detail previously [13,27,28] exerts a small sinusoidal torque (of amplitude $\approx 10^{-3}$ N m) to the end of a cylindrical sample (8 mm in diameter, and 20–30 mm in length). A simple schematic of the device is shown in Fig. 5. The harmonic torque applied to the sample is generated using a pair of electromagnets (two microphone-type coils) connected to a synthesiser via a power amplifier. The sample is fixed between two aligned alumina rods, onto which two sets of light aluminium wings are also attached. The angular deformation across the sample is measured by pairs of capacitive pick-ups which respond to the movement of pure iron plates located at the ends of the aluminium wings. The capacitive signal is detected and amplified using a 5 kHz-frequency bridge which is sampled using a PC. Calibration of the equipment has been described previously [26], with shear modulus measurements being accurate to 2–5% (due to thermal drift of the calibration at high temperatures).

Although the mechanical design of the equipment has not changed from that used previously, the data acquisition hardware and processing software have been improved significantly. For each measurement, data are collected over two periods of the torsional oscillation (Fig. 4). Data are sampled at up to 10 kHz, allowing 1000 signal samples per channel to be acquired at the highest frequency used during experiments (20 Hz). At torsional oscillation frequencies of 2 Hz or lower the number of signal samples per channel is limited to 10 000. Sinusoids are automatically fitted to the collected data using a Levenberg–Marquardt algorithm, and the shear modulus and phase difference between the applied torque and the angular displacement across the sample are calculated from the phase and amplitude parameters of the fitted curves.

Experiments were made over the frequency range 0.002–20 Hz (at $\approx$0.3 log intervals) and at temperatures between $\approx$300 and $\approx$500 °C. The onset of non-linear sample response at temperatures above 490 °C was revealed by the Fourier analysis of the signals indicating the presence of harmonics of the torsional driving frequency.

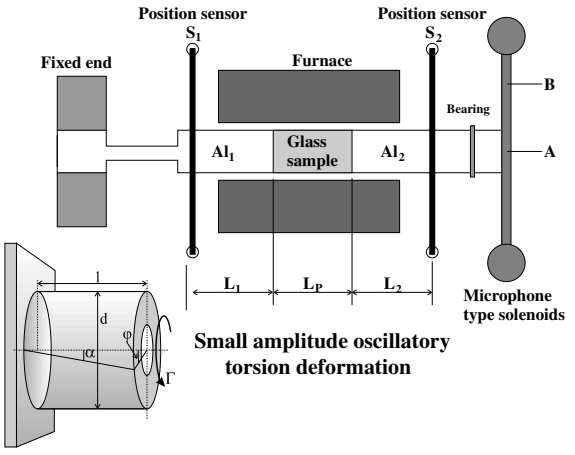

Fig. 4. Principal scheme of the torsion apparatus. The sample under testing was fixed between two rigid Al_2O_3-ceramic rods (Al). One rod was attached to the platform of the device, the second rod was harmonically twisted via a pair of microphone type solenoids.

When the amplitude of the third harmonic of the driving frequency observed in the spectrum of the torsion deformation of the sample was >2–3%, the experiments were stopped. Automation of sampling and processing allows repeated measurements and at high frequencies an average of twenty measurements was used for most temperature–frequency points. At frequencies below 0.05 Hz, individual measurements take up to 17 min, so fewer experiments are averaged.

During experiments the furnace was purged with a flow of Ar gas (5 $cm^3 s^{-1}$). Temperatures were recorded using Cromel–Alumel (K-type) thermocouples. Direct measurements of the temperature field inside the furnace between 300 and 500 °C indicated that temperatures were reduced by up to 5 °C at a distance of 15 mm from the hottest point. Although this spatial sensitivity implies that recorded values were only accurate to $\approx$5 °C as indicators of the sample temperature, relative temperature changes within any one experiment are much better ($\pm$1 °C at 500 °C).

The data collected during slow stepwise heating of the sample allowed calculation of the magnitude of the complex shear modulus $G^*(\omega, T)$, and the phase shift $\varphi(\omega, T)$ between the applied torque and the resultant angular strain of the sample, where

ω is the angular velocity (equal to 2π multiplied by the applied frequency). Before starting the measurement, the sample was kept at each temperature for 2–3 h in order to avoid the effect of heating rate on the shear modulus [2], but still fast enough to exclude measurable amount of metastable phases nucleated during this time [29]. At temperatures above 465 °C, the experiments were shorter than ≈1 h in order to avoid the nucleation of new crystals. From the results of $G^*(\omega, T)$, the real, G', and the imaginary, G'', parts of the complex shear modulus, the internal friction, Q^{-1} and the complex shear viscosity, η, can be calculated from [3]

$$G^* = G' + \mathrm{i}G'' = |G^*|\cos(\varphi) + \mathrm{i}|G^*|\sin(\varphi), \tag{1}$$

$$Q^{-1} = \tan(\varphi) = \frac{G''}{G'}, \tag{2}$$

$$\eta = \eta' - \mathrm{i}\eta'' = \frac{G''}{\omega} + \mathrm{i}\frac{G'}{\omega}. \tag{3}$$

The zero-rate shear viscosity (macroscopic viscosity), η_0 and recoverable compliance, J^0 (which relates to elastic recovery after deformation) may be obtained from the frequency dependence of G' and G'' by [2]

$$\eta_0 = \lim_{\omega\to 0}\frac{G''(\omega)}{\omega}, \tag{4}$$

$$J_0 = \lim_{\omega\to 0}\frac{G'(\omega)}{[G''(\omega)]^2}. \tag{5}$$

From Eqs. (4) and (5) the maximum relaxation time, $\tau_{\max}$, which provides the time-scale for completion of deformation after flow, may be given by the product $\eta_0 J_0$ [2]. If the parameters η_0 and J_0 are frequency dependent at low frequency limit, then the viscoelastic behaviour of material is more complex than a Maxwell body, and a new differential relation must be found for stress and strain (e.g. [28]).

2.4. Sample bonding

During experiments it is essential that each end of the sample is securely bonded to the alumina rods. In order to do this efficiently small conical grips (angle ≈1°, length 4 mm, Fig. 3) were machined at both flat ends of the sample with a diamond tool. Complementary mating grips were produced in the alumina rods and samples were cemented between the rods with a high temperature cement. The assembly was placed in the torsion apparatus and the sample was then bonded to the rods for 2 h at 150 °C and then for 24 h at 400 °C, under an axial load of ≈8 N (e.g. [13]). Measurements carried out using a dummy sample of Al_2O_3 demonstrated that the effect of the cement on phase delay measurements was less than 5×10^{-4} rad.

2.5. Size and shape factors

During heating, the thermal expansion of the sample and the alumina ceramic rods was accommodated by a spring located at one end of the apparatus. At temperatures sufficiently high for the sample to deform, some of the accumulated stress dissipates by flow shortening of the sample. Changes in sample length were calculated from micrometer readings taking at the spring (to a precision of ≈0.02 mm) and corresponding changes in the sample diameter (calculated by assuming conservation of sample volume) were then used to calculate the material properties. However, samples recovered after experiments have shown that flow deformation is not continuously distributed through the samples but concentrates in the centre, producing distorted, barrel-shaped, cylinders. This is a consequence of temperature gradients across the sample and because it was supported at both ends. Thus, despite efforts to account for changes in the sample shape, the deviation from a cylindrical form introduced errors in the assumed diameter of the sample once sample shortening has started (≈1–2%). Calibration of the apparatus allows the conversion of the voltage amplitudes into values of maximum torque and angular displacement. For this purpose a set of small static weights were loaded on a pivotal wing of the torsion apparatus and the static angle deformation of the mechanical system has been measured as a static electric signal and compared with the static mechanical angle deformation of the sample measured from two displacement gauges. These values in turn are used to calculate the complex

shear modulus of the sample. During oscillation experiments the mechanical gauges were dismounted (for more details see [27]). The software can perform a single run or, more usually, a series of runs (e.g. 10 lots of two periods) and provide average results with an associated standard deviation. A micrometer is used to record longitudinal thermal expansion and the subsequent flow shortening of the sample at high temperatures.

The complex shear modulus $G^*(\omega)$ determined in the torsion experiments on a cylindrical sample, on which a small linear angle deformation $\alpha(\omega)$ is exerted, is as follows:

$$|G^*(\omega)| = \frac{32Tl_p}{\pi d_p^4 \alpha(\omega)}, \tag{6}$$

where T is the torque, l_p is the length of the sample, d_p is the diameter of the sample and $\alpha(\omega)$ is the twist angle of the sample deformation (e.g. [27]).

3. Results

The results are presented in Fig. 5 as plots of the real and imaginary components of complex shear modulus, G^*. The data shown demonstrate the difference in the behaviour of shear modulus at temperatures below and above the T_g of the glass matrix (≈440–445 °C), although data were actually collected at temperature intervals of 10 °C. At temperatures below T_g, the data yield a frequency independent value of unrelaxed shear modulus G_∞, given in Table 1. Crystal content results in the increase of the unrelaxed shear modulus of Li_2O–$2SiO_2$ glasses: in the sample with ≈27 vol.% of crystals the shear modulus is 3% greater than in the glass without crystals. The maximum of the imaginary component of shear modulus shifts toward high frequency with the temperature increase. The activation energy of this peak calculated by using the Arrhenius equation are indicated in Table 1.

The frequency dependence of the real component of the dynamic shear viscosity $\eta'(\omega)$, as calculated from the $G^*(\omega)$ data and Eq. (3) is shown in Fig. 6. With decreasing frequency of oscillations the calculated real component, $\eta'(\omega)$, tends to a

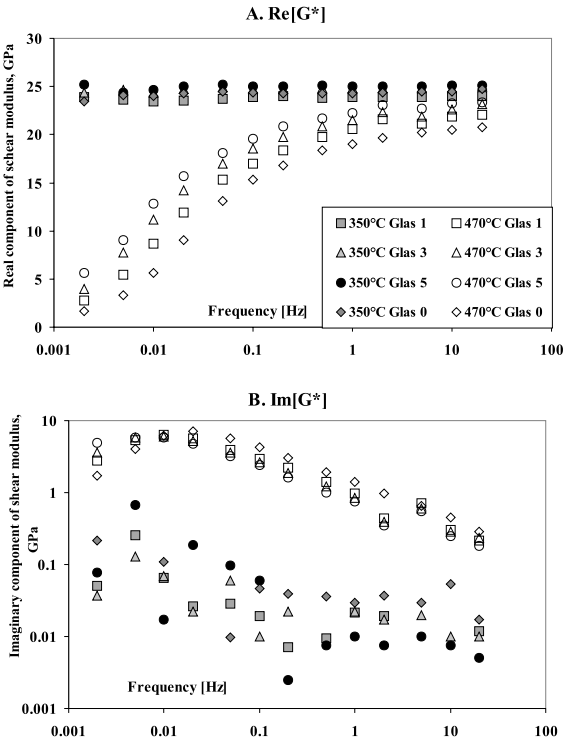

Fig. 5. Real (upper panel) and imaginary (lower panel) components of complex shear modulus as a function of frequency. Samples with differing crystal content appear to have a different 'effective' rheological glass transition temperature. The maximum of imaginary component of shear modulus for samples with differing crystal content corresponds to different frequencies (lower panel), implying that the onset of a viscous regime shifts toward higher temperatures with increasing crystal content.

certain strain rate independent value η_0 (see Eq. (4)). This relaxed value of shear viscosity depends on temperature. From our data it was possible to estimate the relaxed shear viscosity for two temperatures, 470 and 480 °C using a Cross model. If the material has a strain rate dependent rheology, then two different viscosities, η_0 and η_∞, can be assigned, which relate to the low and high strain rate limits respectively. Assuming $\eta_0 \gg \eta_\infty$, the Cross model gives the viscosity as

$$\eta'(\omega) = \frac{\eta_0}{1 + (\tau\omega)^n}, \tag{7}$$

where τ is an effective relaxation time at a specific temperature and n, where $n < 2$, is a parameter characterising the deviation from a Maxwell type

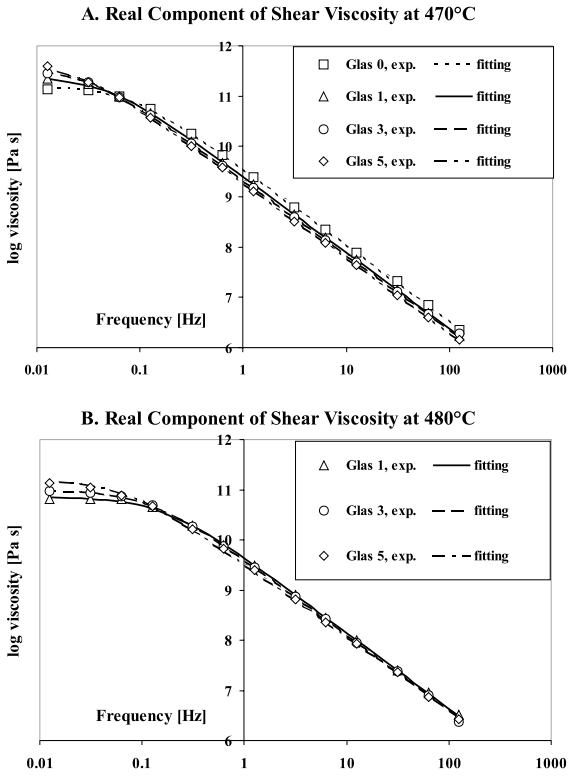

Fig. 6. Experimentally determined shear viscosity at 470 °C (A) and 480 °C (B). From the complex shear modulus data the complex shear viscosity can be obtained as: $\eta(\omega) = \eta'(\omega) - i\eta''(\omega) = \frac{\mathrm{Im}[G^*(\omega)]}{\omega} - i\frac{\mathrm{Re}[G^*(\omega)]}{\omega}$ the extrapolated Newtonian values of shear viscosity were done by the use of the fitting to Eq. (7). Newtonian viscosity is a finite limit of $\mathrm{Re}[\eta(\omega)]$ as $\omega \to 0$. The estimated value of Newtonian viscosity for a glass sample without crystals was used as a normalisation factor for other glass samples.

of the viscoelastic behaviour (represented by $n = 2$, e.g. [30]). By applying Eq. (7) to the data presented in Fig. 6 the relaxed shear viscosity, η_0, for glasses with differing crystal content has been estimated (see Table 2).

In order to reduce the shear modulus and internal friction data obtained at different frequencies and temperatures to a single master curve, a normalised frequency, $\omega\tau$, has been used, where τ is the shear stress relaxation time at a temperature T. The functional dependence of τ with temperature has been chosen to be in the form of an Arrhenian equation as follows:

$$\tau = \tau_0\left(-\frac{E_a}{RT}\right), \tag{8}$$

where τ_0 is a fitting constant and E_a is the activation energy obtained from the fitting of the shear modulus data. The viscoelastic transition in Li_2O–$2SiO_2$ system occurs over a rather short temperature range and the operational frequency window in these experiments was only 4 decades. Thus, the data do not permit the application of a more sophisticated temperature dependence, for example the Vogel–Tammann–Fulcher equation (e.g. [10]). The fitting procedure of τ_0 in Eq. (8) was performed in a way to obtain a single master curve with a minimum sum of square root deviations of single points $\mathrm{Re}[G^*]$ and $\mathrm{Im}[G^*]$. The fitting parameters of a shift factor τ_0 are listed in Table 1.

In applying this procedure, we tacitly assume a Newtonian rheology for the samples above the glass transition temperature, or the existence of a strain rate independent viscosity at $\omega \approx 0$ (Fig. 6), which has been demonstrated with the sample of zero crystal content in our experiments. By using a normalised frequency and the value of unrelaxed shear modulus G_∞, normalised imaginary and real components of shear modulus $\mathrm{Re}[G^*]$, $\mathrm{Im}[G^*]$

Table 2
Fitting parameters of Eq. (8) for Li_2O–$2SiO_2$ glass samples

Sample no.	Φ (vol.%)	Temperature (°C)							
		470				480			
		$\log(\eta_0)$ (Pa s)	n	τ (s)	τ^* (s)	$\log(\eta_0)$ (Pa s)	n	τ (s)	τ^* (s)
Glass 0	0	11.21	1.51	30.58	6.3	–	–	–	1.8
Glass 1	17	11.40	1.51	68.27	11.7	10.85	1.51	10.36	3.0
Glass 3	22	11.60	1.48	129.85	15.1	10.98	1.50	15.83	4.0
Glass 5	27	11.69	1.49	177.06	22.2	11.21	1.44	34.71	6.5

Mean relaxation time estimated from a Maxwell relationship $\tau^* \approx \eta_0/G_\infty$.

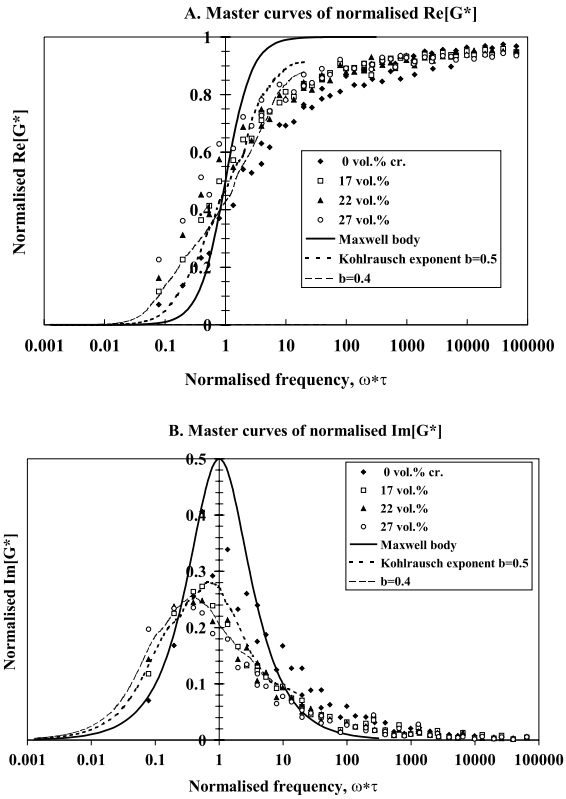

Fig. 7. (A) Real components of shear modulus. With the increase of volume content of crystals in samples the scaling factor of the normalised frequency $\tau = \tau_0 \exp(-E_a/RT)$ increases. This indicates a similar relaxation spectra for all samples, the shape of which evidently differs from a Maxwell body spectrum (solid line), corresponding to a Debye function $\mathrm{Re}[G] = \omega^2\tau^2/(1+\omega^2\tau^2)$ [3]. The transition from elastic to viscous behaviour of Li_2O–$2SiO_2$ glasses occurs over a wider range of $\omega\tau$ in comparison with a Maxwell body. The wideness of the viscoelastic transition is evidence of a certain distribution of shear stress relaxation times in partially crystallised glasses. (B) Imaginary component of shear modulus. With increasing volume content of crystals in the samples, the maximum of $\mathrm{Im}[G^*]$ is decreases slightly. The main difference in relaxation spectrum between samples with differing crystal content is mainly due to a shift factor of the normalised frequency $\omega\tau$. The solid line represents a Debye function $\mathrm{Im}[G] = \omega\tau/(1+\omega^2\tau^2)$ [3]. From the asymmetric and extended (towards high frequencies–low temperatures) shape of the normalised $\mathrm{Im}[G(\omega\tau)]$ the relaxation time spectrum can be inferred.

(Fig. 7), and internal friction Q^{-1}, obtained from Eq. (2) (Fig. 8), were plotted as function of normalised $\omega\tau$. The resulting master curves can be used to characterise the way in which the visco-

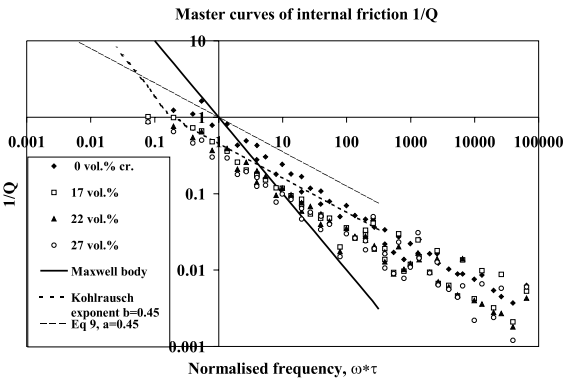

Fig. 8. Master curve of Q^{-1}. The slope of Q^{-1} in a double logarithmic plot as a function of $\omega\tau$, is a measure of the wideness of the stress relaxation time distribution. From our data, the slope n of $Q^{-1} \approx 1/(\omega\tau)^{\alpha}$ is similar for all glass samples, at $\alpha \approx 0.45$, reflecting the similar shape of the relaxation spectra. The solid line is a slope corresponding to the exponential relaxation law of a Maxwell body $Q^{-1} \approx 1/\omega\tau$.

elastic transition, as indicated by $\mathrm{Re}[G]$, $\mathrm{Im}[G]$ and Q^{-1}, differs from that of an ideal viscoelastic transition, i.e. that of a Maxwell body [3]. Normalised frequency dependence of real and imaginary components of shear modulus for a Maxwell body are described by Debye functions and are plotted in Figs. 7 and 8 as a solid line. Evidently, the observed viscoelastic transition in Li_2O–$2SiO_2$ partially crystallised glasses is different from Maxwell-body dependencies of shear modulus and internal friction on a normalised frequency. Relaxation of the shear modulus occurs in a wider range of normalised frequency $\omega\tau$. The deviation from a Maxwell body relaxation or Debye type functions may characterised with an exponent n as follows:

$$Q^{-1} = \frac{1}{(\omega\tau)^{\alpha}}. \tag{9}$$

On a double log scale plot, the data of $Q^{-1}(\omega\tau)$ fit a straight line with a slope $\alpha \approx 0.45$ (Fig. 8).

4. Discussion

4.1. Width of viscoelastic transition in glasses

The simplest relaxation model, which assumes a single relaxation time (Maxwell body) and

stochastic dynamics fails to explain the observed frequency dependence of the peak of imaginary components of shear modulus in Li_2O–$2SiO_2$ glasses (Fig. 7(B)). The half width of the $\mathrm{Im}[G^*]$ peak for the Maxwell body is 1.14 decades, $\mathrm{Re}[G^*]$ varies from unrelaxed to relaxed values in the same width of normalised frequencies [3]. The observed half width of $\mathrm{Im}[G^*]$ for lithium disilicate glasses is about 2–2.1 decades of the normalised frequency and about 1.5 times broader than Debye peak (Maxwell body relaxation) and does not depend on the crystal content, but at the same time the normalised frequency range over which the $\mathrm{Re}[G^*]$ varies from unrelaxed (high frequency limit) to relaxed (low frequency limit) values, is about 4–5 decades and becomes broader with the crystal content increase. This extended shoulder of high frequency–low temperature relaxation is ascribed to a stretched exponential relaxation in glasses [31]. The physical background of the non-Debye relaxation in silicate glasses has been discussed by many authors and it is beyond the scope of this work (e.g. [32–34]). It is worth to note here that estimating the fractional exponent which appears in the stretched exponential relaxation (a Kohlrausch exponent b) is not so straightforward from the experiments. For example, from Fig. 7(B) the maximum of $\mathrm{Im}[G^*]$ is about 0.3 for a sample with 0 vol.% of crystals, 0.27 for 17 vol.%, and about 0.25 for 22–27 vol.%. It may be concluded that a Kohlrausch exponent decreases with a crystal content increase. However, the half width of $\mathrm{Im}[G^*]$ is the same for all four glasses. Judging from the amplitude of the $\mathrm{Im}[G^*]$ peak the rough estimation of a Kohlrausch exponent is $b \approx 0.55$ for 0 vol.%, ≈ 0.45 for 17 vol.%, ≈ 0.4 for 22–27 vol.%, which corresponds to numerically calculated $\mathrm{Im}[G^*]_{\max}$ of ≈ 0.3, 0.266 and 0.254, respectively [26]. It should be noted here that this tendency can be derived from comparing of only one parameter of relaxation curves. The shape of $\mathrm{Im}[G^*]$ (Fig. 7(B)) of samples with differing crystal content is alike, implying the same shape of relaxation spectra and the same exponent (≈ 0.45) for the relaxation model in the first approximation, independent of crystal content. The only difference in $\mathrm{Im}[G^*]$ between glasses with differing crystal content is a shift of the Debye peak as function of normalised frequency, reflecting the fact of a relative τ increase with the increase of crystallinity.

The broadness of the viscoelastic transition may be a result of a non-exponential decay law for silicate glasses with a single 'effective' relaxation time or it may be a superposition of a set of exponentially decaying processes. In this case the relaxation functions of $\mathrm{Re}[G^*]$ and $\mathrm{Im}[G^*]$ may be calculated, if the relaxation spectrum or distribution of relaxation times $H(\tau)$ is known [3]. Assuming that the observed $\mathrm{Re}[G^*]$ and $\mathrm{Im}[G^*]$ for lithium disilicate glasses correspond to a stretched exponential relaxation b, the relaxation spectrum can be calculated as follows:

$$H(\tau) = \frac{1}{\pi}\int_0^\infty \exp(-z)\left(\exp\left(-\left\{\cos(\pi b)\left(z\frac{\tau}{\tau^*}\right)^b\right\}\right)\right)\sin\left(\sin(\pi b)\left(z\frac{\tau}{\tau^*}\right)^b\right)\mathrm{d}z, \tag{10}$$

where τ^* is a mean relaxation time determined from the relaxed shear viscosity and unrelaxed shear modulus of a sample at a given temperature and crystal content (Table 2), and z is a variable of the integration [35]. Eq. (10) implies an exponential stress relaxation function. From $\mathrm{Im}[G^*]$ measurements in this study (Fig. 7(B)) the power law estimated from the half width of $\mathrm{Im}[G^*]$ peak and compared with those calculated for the stretched exponent model provides the estimation of $b \sim 0.45$. The results of generated spectra by the use of Eq. (10) with a parameter $b = 0.45$ are shown in Fig. 11.

A different expression for the relaxation spectrum may be derived for a body with a power-law Q^{-1} dependence on frequency [36]. The data of Q^{-1} presented in Fig. 8 implies a power-law behaviour with a power law exponent α constant over a wide range of normalised frequency, $\omega\tau$. In comparison, a stretched exponential relaxation with $b \approx 0.45$ the internal friction Q^{-1} depends on $\omega\tau$ in a different way. At high frequencies–low temperatures, $Q^{-1} \approx 1/(\omega\tau)^{0.45}$, for $\omega\tau \geqslant 0$ the internal friction $Q^{-1} \approx 1/(\omega\tau)$ [26]. The observed power law dependence of the internal friction implies that the

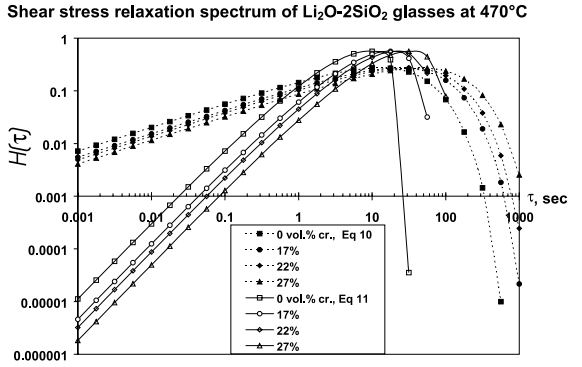

Fig. 9. The calculated spectrum of shear stress relaxation based on Eqs. (10) and (11) corresponding to the stretched exponential relaxation (dotted lines) and a power-law Q^{-1} (solid lines). The mean relaxation time has been estimated from the Maxwell relationship $\tau^* \approx \eta_0/G_\infty$ (Table 2).

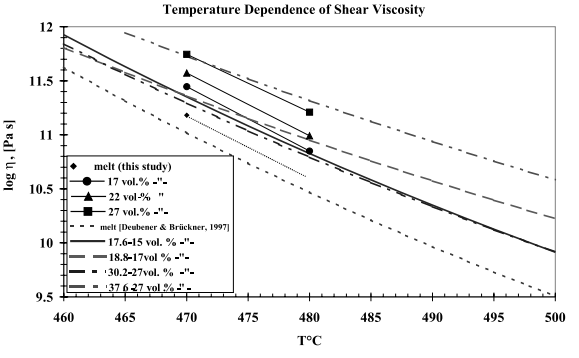

Fig. 10. The measured relaxed shear viscosity of partially crystallised Li_2O–$2SiO_2$ glasses in comparison with the compression experiments of Deubener and Brückner [10]. The small difference in shear viscosity may be due to the two different types of the deformation experiments. The torsion experiments in this study directly provides relaxed (strain rate independent) shear viscosity. In measurements of shear viscosity from compression experiments [10] it is assumed that the volume viscosity of samples is infinite.

relaxation in lithium disilicate glasses is different from the stretched exponential relaxation. For the relaxation model of a body with a power law dependence α, the relaxation spectrum for $\tau < \tau^*$ can be written as follows [36]:

$$H(\tau) = 2.46\left(\frac{\tau}{\tau^*}\right)\sin\left[2\cos\left(\alpha\frac{\pi}{2}\right)\left(\frac{\tau}{\tau^*}\right)^{\alpha}\right] \exp\left[-\frac{1}{\sin(\alpha(\pi/2))}\left(\frac{\tau}{\tau^*}\right)^{\alpha}\right]. \quad (11)$$

The numerical constant has been chosen in order to produce an area below the curve equal to that produced by curves generated from Eq. (10). The calculated spectra of the partially crystallised glass samples of Li_2O–$2SiO_2$ with $\alpha = 0.45$ are shown in Fig. 9. The comparison of two sets of spectra indicates that the relaxation spectrum of a body with a power law dependence on frequency has narrower band of relaxation times centred around a mean value τ^*. This correlates with the observed relatively narrow half width of $\mathrm{Im}[G^*]$ in comparison with the case of a stretched relaxation.

4.2. Relaxed shear viscosity

The relaxed shear viscosity of all glasses measured in this study are presented in Fig. 10, and are in satisfactory agreement with the data from the compression experiments of Deubener and Brückner [10]. In this study we examined the effect of crystals on the internal friction and shear viscosity of Li_2O–$2SiO_2$ glasses. The increase in viscosity with crystal content is approximately $+0.2\log(\mathrm{Pa\,s})/10$ vol.%. This corresponds to an increase of the rheological T_g by approximately $+3.8$ °C/10 vol.%. Among other factors influencing the variation of viscosity or T_g and Q^{-1} are non-stoichiometry of glass composition, water content and cooling rate during the preparation of samples.

Water dissolved chemically in silicate glasses breaks the network Si–O bonds. Even a few ppm of dissolved water may affect the internal friction and shear viscosity of silicate glasses. In lithium disilicate glasses containing OH-species protons are attached to non-bridging oxygens and, therefore, affect the mechanical damping [5]. In previous studies on lithium silicates and other alkali silicates it was noticed that with the increase of the OH-species content the activation energy of the high temperature internal friction peak decreases and the peak shifts to lower temperature. DSC measurements of water bearing lithium disilicate glasses indicate a decrease of $T_g \approx -17$ °C/1000 ppm of water content [17], which corresponds to the viscosity decrease approximately $-1.03\log(\mathrm{Pa\,s})/1000$ ppm. In comparison, the

effect of variations in cooling rate is approximately +13.5 °C/log(K min^{-1}) obtained from DSC [17] and approximately +35.6 °C/log(K min^{-1}) obtained from DTA [16]. These variations in T_g imply a significant increase in the shear viscosity with an increasing cooling rate from +0.8 to +1.93 log(Pa s)/log(K min^{-1}), respectively. The effect of the chemical composition on T_g is much smaller approximately +3.5 °C/10 mol% of Li_2O [14], which corresponds to +0.2 log(Pa s)/10 mol% of Li_2O. Thus, the observed tendency of the viscosity increase cannot be explained by the small deviations of the chemical composition of glasses from stochiometric composition, uncertainty in cooling rates or few ppm of water content.

The relative variations of the shear viscosity between samples with differing crystal content (Φ) correlate with estimations obtained with the use of the Einstein–Roscoe equation

$$\eta_{rel} = \left[1 - \frac{\Phi}{\Phi_{cr}}\right]^{-m}, \qquad (12)$$

where η_{rel} is a shear viscosity of a suspension scaled to the shear viscosity of a melt, Φ_{cr} is a concentration of close packing [37]. At a dilute concentration limit Eq. (12) may be approximated as $\approx 1 + m(\Phi/\Phi_{cr})$. Eq. (12) has been derived for a suspension of spherical particles uniform in size, and theoretically $\Phi_{cr} = 0.74$ in the case of ideal close packing. If the exponent $m = 2.5$ is fixed, the data of the relative viscosity fit Eq. (12) yielding $\Phi_{cr} = 0.72$ (see Fig. 11). In the case of a suspension of oblated spheroids the exponent $m = 2.5$ as well as Φ_{cr} must be replaced by functions of the aspect ratio of ellipsoids. For example, in the case of lithium disilicate crystals (aspect ratio of axes 1:1:1.7) the coefficient in Eq. (12) for the dilute approximation must be about 2.7 [38]. The critical concentration depends in turn on the aspect ratio of particles and their size distribution. From experiments with monodisperse particles of a uniform size $\Phi_{cr} = 0.605$ [39], which corresponds to so called random close packing. Essentially, the maximum packing parameter may vary between 0.605 and 0.85 depending on the diameter ratio of smallest and largest particles in the [40]. For a given aspect ratio of lithium disilicate crystals the close packing parameter may be estimated as $\Phi_{cr} \approx 0.65$. At this given value of the close packing parameter and the value 2.7 in the linear approximation of Eq. (12) for a dilute suspension case, the estimated value $m \approx 1.76$ provides a satisfactory agreement with the measured data of η_{rel} (Fig. 11). The general analysis of experimental data for suspensions in viscous liquids indicates that, for smooth spherical particles, $m \approx 2$ and $\Phi_{cr} \approx 0.66$–0.44 in the range of particle aspect ratios 1–8 [41]. Assuming $m = 2$, the best fit to the data obtained in this study is with $\Phi_{cr} = 0.65$. Alternatively, Chong et al. [39] suggested an equation for the rheology of concentrated suspensions as follows:

$$\eta_{rel} = \left[1 + 0.75\frac{\Phi/\Phi_{cr}}{1 - \Phi/\Phi_{cr}}\right]^2. \qquad (13)$$

The data obtained in this study may satisfy Eq. (13) if $\Phi_{cr} \approx 0.53$, which is too small for a random close packing parameter. Fig. 11 represents the comparison of the shear viscosity data measured in this study with three cases of Eq. (12) and best fit with Eq. (13). The agreement is poor in the case of high crystallinity ($\Phi \approx 27$ vol.%). One of the possible reasons is the development of Bingham be-

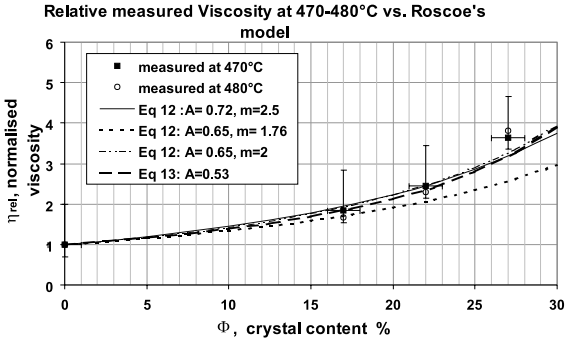

Fig. 11. The Einstein–Roscoe equation and measured relaxed viscosities of partially crystallised Li_2O–$2SiO_2$ glasses. Eq. (12) has been plotted for $\Phi_{cr} = 0.72$ (in the legend $A = \Phi_{cr}$) and exponent 2.5, for $\Phi_{cr} = 0.65$ and exponent 1.76, for $\Phi_{cr} = 0.65$ and exponent 2. Eq. (13) is plotted using $\Phi_{cr} = 0.53$. The data of the relative viscosity measured in the sample with ≈27 vol.% of crystals can not be fitted with the same parameters of Roscoe equation as the data obtained in samples with smaller volume fraction of crystals. One of the possible reasons may be a Bingham behaviour of partially crystallised glasses when crystal content is close to the 'touching limit' ≈28 vol.% [42].

haviour, or the occurrence of a finite yield strength with the increasing volume fraction of crystals. Recent numerical calculations demonstrated that in a suspension of oblated ellipsoids with an aspect ratio 1:1:1.7 the Bingham stress starts to play a role at $\Phi \approx 28$ vol.% when a touching limit of crystal-melt suspension is achieved [42].

5. Conclusions

(1) Non-Debye character of shear modulus relaxation in partially crystallised Li_2O–$2SiO_2$ glasses has been observed by using torsional oscillatory and small strain deformations. Deviations from a Maxwell body viscoelastic behaviour have been characterised by using master curves of $\mathrm{Re}[G^*]$ and $\mathrm{Im}[G^*]$. A power law for internal friction with an exponent of 0.45 is characteristic for partially crystallised samples and a pure glass. The broadened relaxation spectrum does not depend on crystal content and is entirely due to the extended mechanical relaxation spectrum of the Li_2O–$2SiO_2$ glass matrix.

(2) The effect of crystal content on shear modulus is minor; it affect only few percent of the unrelaxed shear modulus. The temperature background of the internal friction is characterised by an Arrhenian equation with an activation energy of ≈135–120 kJ/mol, which is close to the diffusion activation energy of non-bridging oxygen. In glasses with differing crystal content, master curves of shear modulus relaxation are similar but shifted in a normalised frequency scale by a factor proportional to the effective shear viscosity.

(3) The effect of crystals on shear viscosity of Li_2O–$2SiO_2$ glasses containing up to 30 vol.% of crystals is $0.2\log(\mathrm{Pa\,s})/10$ vol.%. The rheology of Li_2O–$2SiO_2$ suspensions may be fitted to a Einstein–Roscoe equation when the crystal content <25 vol.%. At higher concentrations, a Bingham strength of the suspension may cause deviation from Einstein–Roscoe dependency.

References

[1] C.A. Wert, J. Appl. Phys. 60 (1986) 1888.
[2] G. Marin, Oscillatory rheometry, in: A.A. Colyer, D.W. Clegg (Eds.), Rheological Measurement, Chapman and Hall, London, 1998, p. 3.
[3] A.S. Nowick, B.S. Berry, Anelastic Relaxation in Crystalline Solids, Academic Press, NY, 1972.
[4] I.L. Hopkins, C.R. Kurkjian, in: Physical Acoustics. Principles and Methods. 2, part B, Academic Press, London, 1965, p. 91.
[5] W.A. Zdaniewski, G.E. Rindone, D.E. Day, J. Mater. Sci. 14 (1979) 763.
[6] K. Sakai, K. Takizawa, T. Eguchi, J. Horie, J. Mater. Sci. Lett. 14 (1995) 1126.
[7] J.A. Lee, R.F. Cooper, J. Am. Ceram. Soc. 89 (1997) 2917.
[8] G. Pezzotti, K. Ota, Scripta Mater. 36 (1997) 481.
[9] N.S. Bagdassarov, Phys. Chem. Mineral. 26 (1999) 513.
[10] J. Deubener, R. Brückner, J. Non-Cryst. Solids 209 (1997) 96.
[11] R. Brückner, J. Deubener, J. Non-Cryst. Solids 209 (1997) 283.
[12] D.E. Day, G.E. Rindone, J. Am. Ceram. Soc. 44 (1961) 161.
[13] H. Berckhemer, W. Kampfmann, E. Aulbach, H. Schmeling, Phys. Earth Planet. Interiors (1982) 29.
[14] V. Braetsch, G.H. Frischat, J. Non-Cryst. Solids 95&96 (1987) 457.
[15] R. Brückner, J. Deubener, M. Sternitzke, J. Non-Cryst. Solids 163 (1993) 1.
[16] K. Cheng, J. Phys. Chem. B 103 (1999) 8272.
[17] M.J. Davis, P.D. Ihinger, J. Non-Cryst. Solids 244 (1999) 1.
[18] H. Kobayashi, T. Kosugi, Y. Kogure, J. Non-Cryst. Solids 179 (1994) 324.
[19] H. Kobayashi, Y. Kogure, T. Kosugi, Physica B 253–264 (1999) 346.
[20] B.S. Lunin, S.N. Torbin, Vest. Moscow Univ. Ser. Chem. 41 (2) (2000) 93.
[21] V.A. Versteeg, D.L. Kohlstedt, J. Am. Ceram. Soc. 77 (1994) 1169.
[22] T. Sakai, M. Eguchi, K. Takizawa, J. Non-Cryst. Solids 185 (1995) 159.
[23] S. Bark-Zollmann, G. Kluge, K. Heide, Glastech. Ber. 71 (1988) 57.
[24] I. Jackson, Annu. Rev. Earth Planet. Sci. 21 (1993) 375.
[25] T.T. Gribb, R.F. Cooper, Rev. Sci. Instrum. 69 (1998) 559.
[26] N. Bagdassarov, Anelastic and viscoelastic behaviour of partially molten rocks and lavas, in: N. Bagdassarov, D. Laporte, A.B. Thompson (Eds.), Physics and Chemistry of Partially Molten Rocks, Kluwer Academic, Dordrecht, 2000.
[27] W. Kampfmann, Master's thesis, J.W. Goethe Universität Frankfurt a. M., Institut für Meterologie und Geophysik, 1980.
[28] N. Bagdassarov, D. Dingwell, S. Webb, Eur. J. Mineral. 5 (1993) 409.

[29] L.L. Burgner, P. Lucas, M.C. Weinberg, P.C. Soares Jr., E.D. Zanotto, J. Non-Cryst. Solids 274 (2000) 188.
[30] H.A. Barnes, J. Non-Netonian Fluid Mech. 81 (1999) 133.
[31] W. Götze, L. Sjörgen, Rep. Progr. Phys. 55 (1992) 241.
[32] J. Jäckle, Philos. Mag. B. 56 (1987) 113.
[33] C.A. Angell, J. Non-Cryst. Solids 131–133 (1991) 13.
[34] A. Sjölander, J. Phys.: Condens. Matter 5 (1993) B201.
[35] A. Muoñz, F.L. Cumbrera, Thermochim. Acta 196 (1992) 137.
[36] G. Müller, J. Geophys. 54 (1983) 20.
[37] R. Roscoe, Brit. J. Appl. Phys. 3 (1952) 267.
[38] L.D. Landau, E.M. Lifschitz, Lehrbuch der theoretischen Physik. Hydrodynamik, Akademie Verlag, Berlin, 1971.
[39] J.S. Chong, E.B. Cristiansen, A.D. Baer, J. Appl. Polym. Sci. 15 (1971) 2007.
[40] T. Dabak, O. Yucel, Rheol. Acta 25 (1986) 527.
[41] A.B. Metzner, J. Rheol. 29 (1985) 739.
[42] M.O. Saar, M. Manga, K.V. Cashman, S. Fremouw, Earth Planet. Sci. Lett. 187 (2001) 367.